



# Adaptive Digital Processing Investigation of DFT Subbanding vs Transversal Filter Canceler

W. F. GABRIEL

*Electromagnetics Branch  
Radar Division*

SECURITY CLASSIFICATION OF THIS PAGE

REPORT DOCUMENTATION PAGE				
1a. REPORT SECURITY CLASSIFICATION UNCLASSIFIED		1b. RESTRICTIVE MARKINGS		
2a. SECURITY CLASSIFICATION AUTHORITY		3. DISTRIBUTION/AVAILABILITY OF REPORT		
2b. DECLASSIFICATION/DOWNGRADING SCHEDULE		Approved for public release; distribution unlimited.		
4. PERFORMING ORGANIZATION REPORT NUMBER(S) NRL Report 8981		5. MONITORING ORGANIZATION REPORT NUMBER(S)		
6a. NAME OF PERFORMING ORGANIZATION Naval Research Laboratory	6b. OFFICE SYMBOL (If applicable) Code 5372	7a. NAME OF MONITORING ORGANIZATION		
6c. ADDRESS (City, State, and ZIP Code) Washington, DC 20375-5000		7b. ADDRESS (City, State, and ZIP Code)		
8a. NAME OF FUNDING/SPONSORING ORGANIZATION Army MICOM and NAVSEASYSCOM	8b. OFFICE SYMBOL (If applicable)	9. PROCUREMENT INSTRUMENT IDENTIFICATION NUMBER		
8c. ADDRESS (City, State, and ZIP Code) Army MICOM/CCM, Adelphi, MD 20783 NAVSEASYSCOM, Washington, DC 20362-5101		10. SOURCE OF FUNDING NUMBERS		
		PROGRAM ELEMENT NO. 63749A 62712N	PROJECT NO. D462-02-AJ3 SF-12-131	TASK NO. WORK UNIT ACCESSION NO. DN115-149 DN480-638
11. TITLE (Include Security Classification) Adaptive Digital Processing Investigation of DFT Subbanding vs Transversal Filter Canceler				
12. PERSONAL AUTHOR(S) Gabriel, William F.				
13a. TYPE OF REPORT Interim	13b. TIME COVERED FROM _____ TO _____	14. DATE OF REPORT (Year, Month, Day) 1986 July 28	15. PAGE COUNT 22	
16. SUPPLEMENTARY NOTATION				
17. COSATI CODES		18. SUBJECT TERMS (Continue on reverse if necessary and identify by block number)		
FIELD	GROUP	SUB-GROUP		
			Adaptive filters	
			Digital processing	
			DFT Subbanding	
			Tapped delay lines	
			Digital filters	
			Transversal filters	
19. ABSTRACT (Continue on reverse if necessary and identify by block number)				
<p>A performance comparison investigation has been carried out for two multiple-weight, adaptive, canceler techniques; the discrete Fourier transform (DFT) band partitioning approach and the transversal filter canceler (TFC) approach. A simple two-channel canceler model was utilized, with all-digital processing, and four different types of channel error were included. For differential delay errors and amplitude/phase ripple errors, the TFC performance is generally far superior to the DFT subband system, for the same number of degrees of freedom. For quadrature errors and sample/hold jitter errors, there was essentially no difference in performance between the two, and performance did not improve as the degrees of freedom were increased. The superior performance of the TFC system is attributed to more effective utilization of its adaptive degrees of freedom and the fact that it is inherently suited to differential delay compensation. The DFT canceler has no differential delay compensation.</p>				
20. DISTRIBUTION/AVAILABILITY OF ABSTRACT <input checked="" type="checkbox"/> UNCLASSIFIED/UNLIMITED <input type="checkbox"/> SAME AS RPT. <input type="checkbox"/> DTIC USERS		21. ABSTRACT SECURITY CLASSIFICATION UNCLASSIFIED		
22a. NAME OF RESPONSIBLE INDIVIDUAL William F. Gabriel		22b. TELEPHONE (Include Area Code) (202) 767-2584	22c. OFFICE SYMBOL Code 5372	

**CONTENTS**

INTRODUCTION.....	1
SINGLE WEIGHT CANCELER .....	4
DFT SUBBAND CANCELER.....	5
TRANSVERSAL FILTER CANCELER.....	13
FURTHER COMPARISON OF DFT VS TRANSVERSAL FILTERS.....	14
CONCLUSIONS.....	18
REFERENCES.....	18

## ADAPTIVE DIGITAL PROCESSING INVESTIGATION OF DFT SUBBANDING VS TRANSVERSAL FILTER CANCELER

### INTRODUCTION

One of the most important and widely used ECCM techniques is the sidelobe canceler (SLC) [1-3]. Although simple in concept and relatively economical in implementation, the SLC performance is limited by a variety of factors, including:

- Multipath delay, often expressed in terms of delay-bandwidth product
- Aperture-frequency dispersion, often expressed in terms of aperture-bandwidth product
- Differing receiver channel responses, often referred to as channel mismatch errors
- Quadrature error in synchronous detectors
- Digital receiver channel errors such as analogue-to-digital (A/D) quantization, sample/hold (S/H) jitter, and dc offset
- Nonlinear effects, intermods, temperature drifts, etc.

To help overcome these limitations, particularly those related to bandwidth, multiple adaptive weight systems have been proposed (over the years) that involve either a tapped delay line transversal filter approach [4-7] or a band-partitioning filter approach such as the discrete Fourier transform (DFT) [8-11]. Despite the fact that both of these multiple-weight adaptive filter approaches are well known, the literature does not have much information that permits a direct performance comparison between the two [11]. Therefore, this report attempts to address that need.

This investigation has been restricted to digital processing systems exclusively because of the computer simulation convenience and, also, because analogue filter systems contain additional errors that would increase the modeling burden. Further, cancellation limitation effects have been investigated by use of a simple two-channel canceler model derived from a typical multichannel receiver system of the type shown in Fig. 1. This system includes radio-frequency (RF) antenna elements and circulators, RF local oscillators (LO), intermediate frequency (IF) amplifiers, synchronous baseband detection with in-phase and quadrature (I&Q) video signal output, baseband video amplifiers with low-pass filters, snapshot sample and hold (S/H) circuits, and analogue to digital (A/D) converters. The output signals consist of digital complex-data (I&Q) samples occurring at a sampling rate related to the Nyquist rate [12].

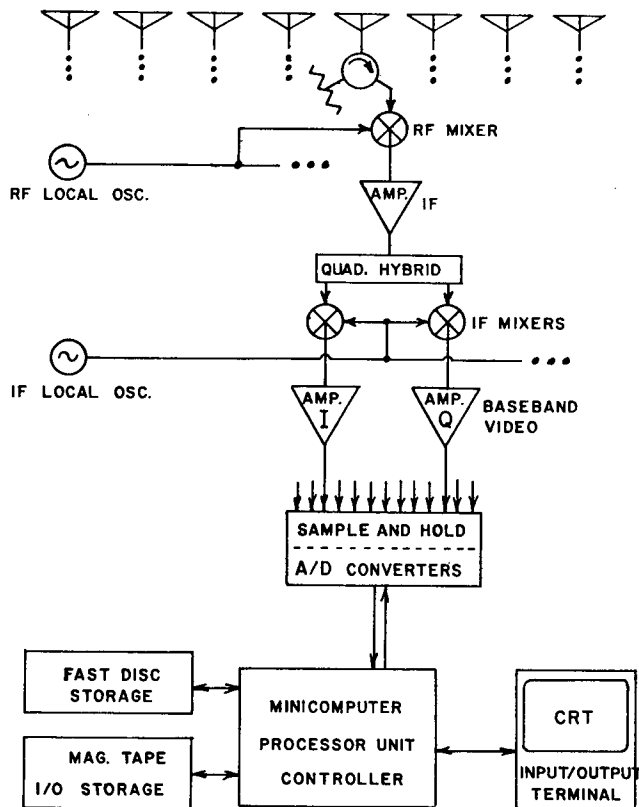


Fig. 1 — Multichannel receiver system feeding digital processor

Figure 2 represents the resultant two-channel canceler model, configured for a single adaptive weight. In this model, we accommodate the insertion of five different types of adaptive processor channel errors:

- Differential delay
- Filter passband ripple errors
- Quadrature error in synchronous detectors
- S/H jitter error
- A/D quantization and offset errors.

Many other types of errors exist in any practical system implementation, but they were not considered in this initial investigation because of time considerations.

A critical choice in any digital data processing system is the particular type of analogue lowpass filter utilized to band-limit the input signal energy without introducing excessive linear or nonlinear distortion. This is a critical operation because in the following stage when the filter's output signal is sampled, any frequencies above one-half the sampling frequency will be folded or "aliased" and appear as signal contributions [12]. In practice, a computer-aided filter design program is often used to produce between a sixth- and eleventh-order design incorporating active filter elements. For the purposes of our simple cancellation performance behavior discussed herein, we assume an ideal Chebyshev 6-pole

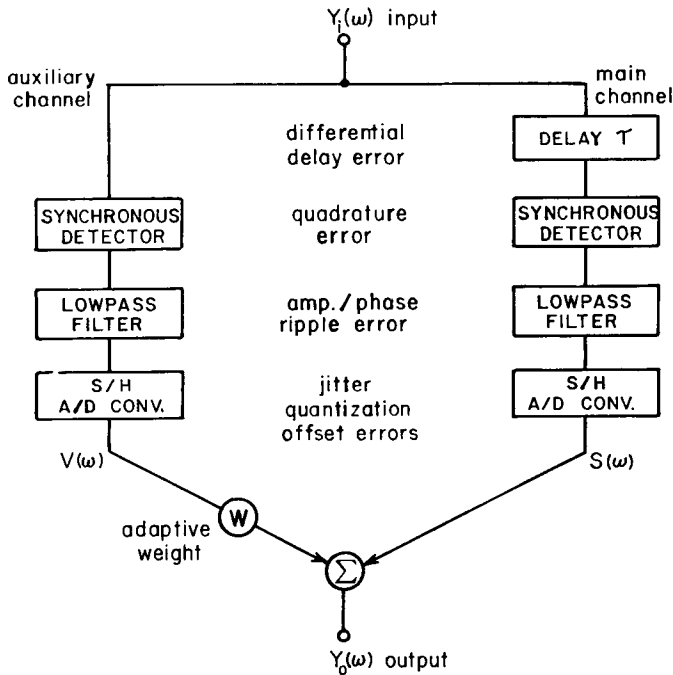


Fig. 2 — Two-channel canceler model with a single adaptive weight

lowpass filter that has a cutoff frequency point selected to be 25% of the sampling frequency. The filter function and its various parameters may be summarized,

$T$  is the sampling period.

$f_s = \frac{1}{T}$  is the sampling rate.

$f_c = 0.25 f_s$  is the lowpass filter "cutoff" frequency.

$\omega = 2\pi (f/f_s)$  is the angular frequency, normalized to the sampling rate

$H(\omega)$  is the filter function.

$$\left[ \frac{1}{|H(\omega)|} \right]^2 = \left\{ 1 + \epsilon^2 \cosh^2 \left[ M \cosh^{-1} \left( \frac{\omega}{\omega_c} \right) \right] \right\} \quad (1)$$

where  $\epsilon^2$  is the lowpass ripple magnitude factor and  $M$  is the number of poles or filter order.

Figure 3 shows a plot of the filter function  $|H(\omega)|^2$  vs angular frequency in  $Z$ -plane degrees, where  $Z = e^{j\omega}$ , computed for  $\epsilon^2 = 0.156$  and  $M = 6$ . Both  $f_c$  and the sharp filter skirt roll-off characteristic were deliberately chosen to give us an "oversampled" system, avoid aliasing problems and yet represent a lowpass characteristic that could be implemented in practice. Recall that the Nyquist rate is half of the sampling rate [12], which equals  $180^\circ$  in the  $Z$ -plane and bounds our frequency plot region.\*

\* Angular frequency  $\omega$  is represented in terms of the complex  $Z$ -plane equivalent,  $Z = e^{j\omega}$ , because of the importance of the  $Z$ -transform in analysis of discrete-time signals and systems [12]. This representation of  $\omega$  involves a natural geometric angle (in degrees), the accommodation of "negative" frequencies, and a clear picture of the periodic/repetitious nature of discrete-time sampled system behavior vs  $\omega$ . For convenience, the term "frequency" is used in place of "angular frequency" throughout the remainder of the report.

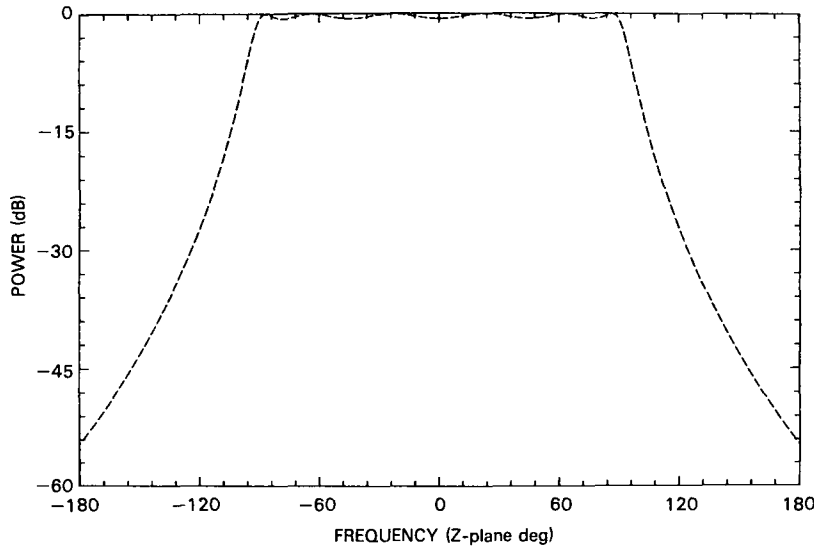


Fig. 3 — Chebyshev 6-pole lowpass filter with 0.25 cutoff point and 0.156 ripple magnitude factor

The representation of filter passband ripple errors in amplitude and phase was chosen to follow the error model described in Ref. 6. Let us define a ripple error function  $E(\omega)$ ,

$$E(\omega) = A(\omega)e^{j\phi(\omega)} \text{ for } |\omega| \leq \left( \frac{\omega_s}{2} \right) \quad (2)$$

where  $A(\omega) = 1.0 + a \cos(c\omega)$ ,  
 $\phi(\omega) = b \cos(c\omega)$ ,  
 $a$  is peak amplitude error,  
 $b$  is peak phase error, and  
 $c$  is cycles of error ripple.

$E(\omega)$  multiplies the filter function in the auxiliary channel to inject the ripple errors; i.e., the main channel is considered the reference here. We assume that  $I$  and  $Q$  lowpass filters in a given channel are identical pairs, such that the error exists only between the two channels.

Quadrature phase error is introduced mainly by the quadrature hybrid circuit that sets up the  $90^\circ$  phase difference for the  $I$  and  $Q$  synchronous video detectors. Figure 4 illustrates the effect, where "Q Signal" denotes the actual position of the  $Q$  axis. The quadrature error  $\xi$  is the deviation of the  $Q$  axis from the true orthogonal  $Y$  axis. The " $I$  Signal" axis is always assumed to be in perfect alignment with the  $X$  axis by definition. Therefore, a true signal vector of magnitude  $\beta$  and phase angle  $\Psi$  is converted by the receiver to another vector,  $\alpha$ , which is in error both in amplitude and phase.

S/H jitter error refers to the uncertainty in the timing of the sampling window when the command is given to sample a signal. For the purposes of this report, we assume that jitter error occurs independently in the  $I$  and  $Q$  signals of both channels, with uniform random distribution.

### SINGLE WEIGHT CANCELER

To gain an initial appreciation for the sensitivity of cancellation degradation to the various types of errors across the filter band, let us review the cancellation performance of the Fig. 2 circuit when single weight  $W = -1$ . The canceler output,  $Y_o(\omega)$ , divided by the input,  $Y_i(\omega)$ , is

$$\frac{Y_o(\omega)}{Y_i(\omega)} = \left( \frac{S(\omega) - V(\omega)}{Y_i(\omega)} \right) \quad (3)$$

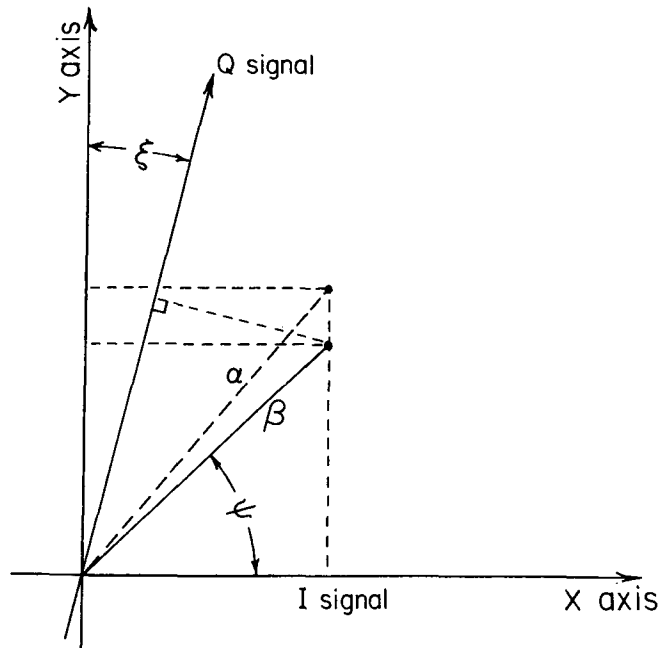


Fig. 4 — Effect of quadrature error on true signal vector

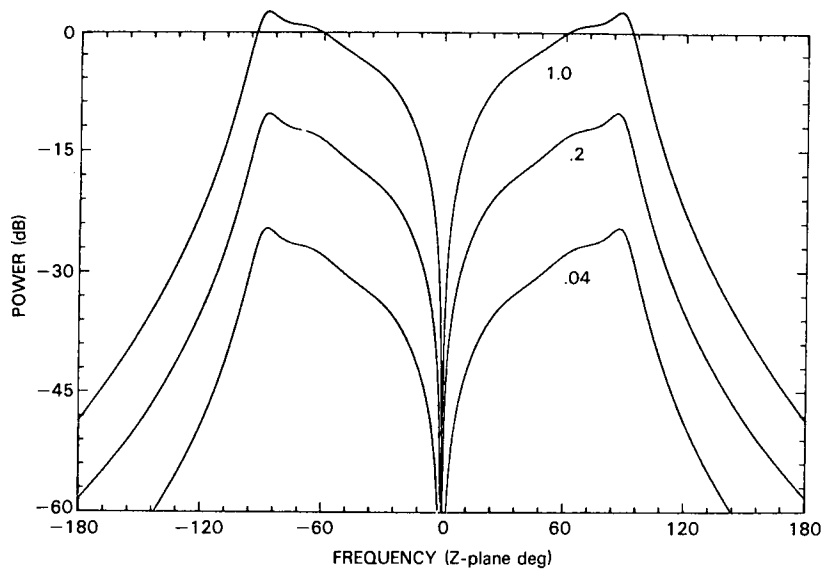
where  $S(\omega)$  and  $V(\omega)$  are the main channel and auxiliary-channel signals being subtracted. Note that if no errors are present in the two channels, then Eq. (3) results in perfect cancellation across the entire filter bandwidth.

Figure 5 illustrates the cancellation degradation for the different types of errors. In Fig. 5(a), delay errors of  $\tau = 0.04, 0.2,$  and  $1.0$  sampling period have been inserted in the main channel, and the response graphically demonstrates that perfect cancellation occurs only at band center; at all other frequencies across the band, the phase error is equal to  $\omega\tau$ . In Fig. 5(b), amplitude ripple error of  $0.1$  peak and  $2.5$  cycles (see Eq. (2)) has been inserted in the auxiliary channel; we note the cyclic behavior in accordance with the ripple, with a peak degradation of  $-20$  dB. The same exact cyclic behavior is produced for a phase ripple error of  $0.1$  radian ( $5.72^\circ$ ) peak. In Fig. 5(c), synchronous detector quadrature errors of  $2.5^\circ$  (rather typical of such circuits) have been inserted in the main and auxiliary channels (total error of  $5^\circ$ ), and we see that cancellation degrades to about  $-21$  dB across the filter passband. Figure 5(d) illustrates the behavior for a jitter error with uniform random distribution between peak values of  $\pm 2^\circ$ , added independently to  $I$  and  $Q$  signals in both channels. Jitter is a delay-type of error and has similar behavior across the passband (compare with Fig. 5(a)).

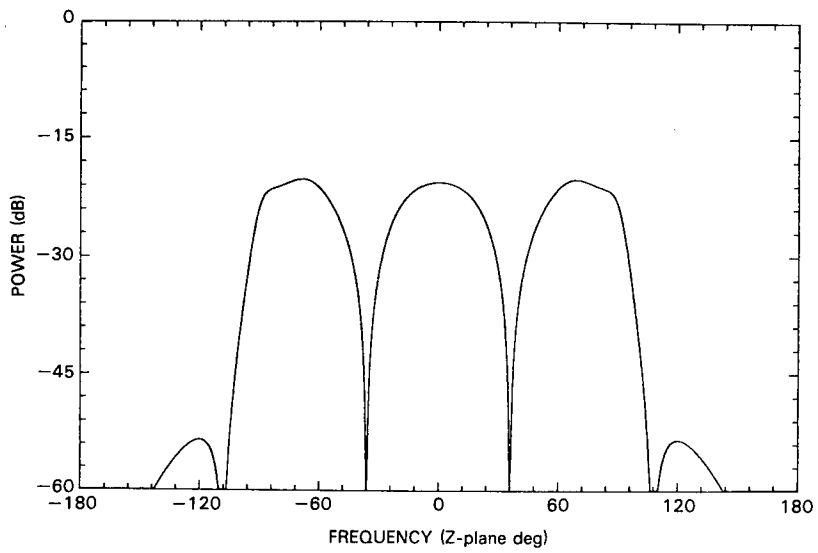
Figure 6 is a universal plot of cancellation in dB vs amplitude or phase errors, based on Eq. (3). It illustrates the considerable precision (small errors) required to achieve large cancellation dynamic ranges.

## DFT SUBBAND CANCELER

One option for extending the single-weight system of Fig. 2 to a multiple-weight canceler is to partition the passband into a number of filter subbands and then provide one adaptive weight for each filter subband [8-11]. A discrete Fourier transform (DFT) filter is a logical method for achieving this band partitioning in a digital processor, and Fig. 7 shows typical subband filter responses for seven taps input/output. The DFT filter requires a sequence of data samples at its inputs, in a manner equivalent

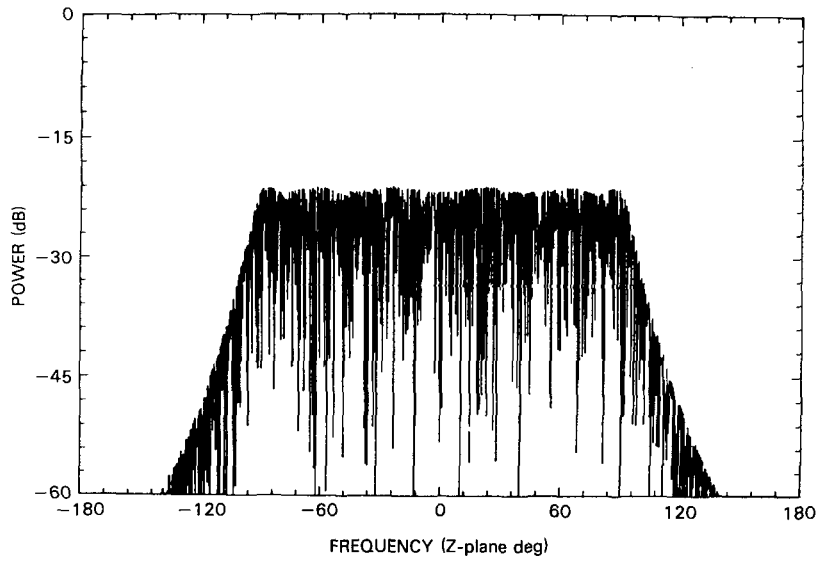


(a) Delay errors of 0.04, 0.2, and 1.0 sampling period

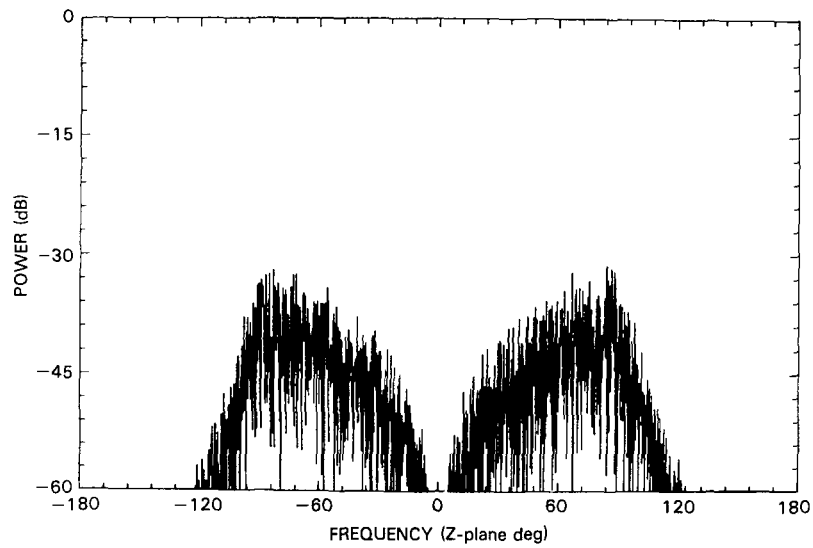


(b) Amplitude ripple error of 0.1 peak and 2.5 cycles

Fig. 5 — Cancellation degradation for various errors, two-channel canceller using single weight of value  $W = -1$



(c) Synchronous detector quadrature error of  $5.0^\circ$



(d) Random jitter error of  $2.0^\circ$  peak, both I&Q

Fig. 5 (Continued) — Cancellation degradation for various errors, two-channel canceler using single weight of value  $W = -1$

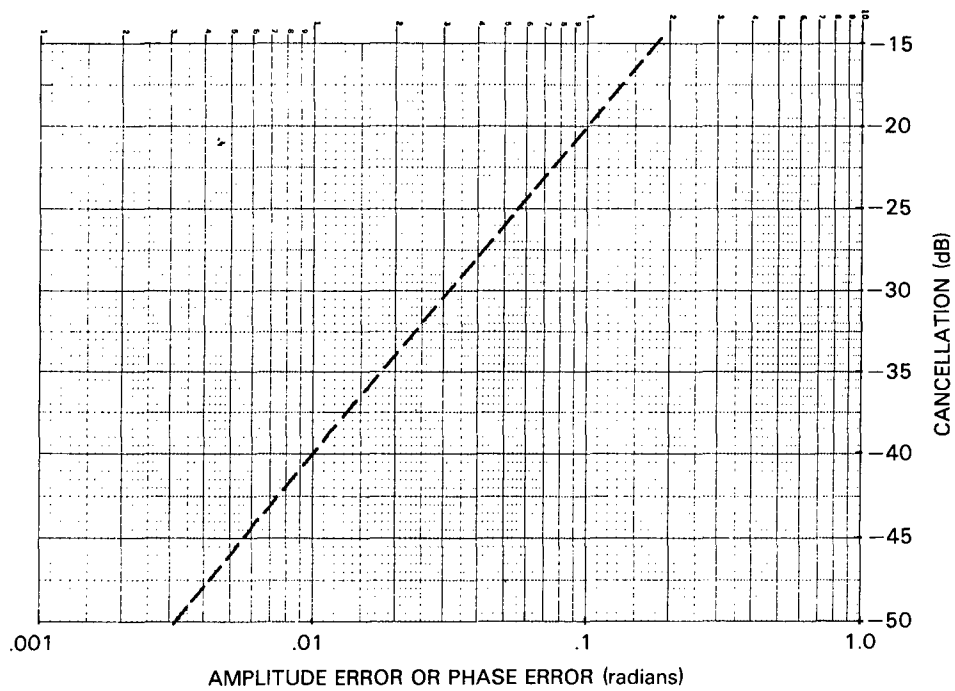


Fig. 6 — Cancellation vs amplitude or phase error

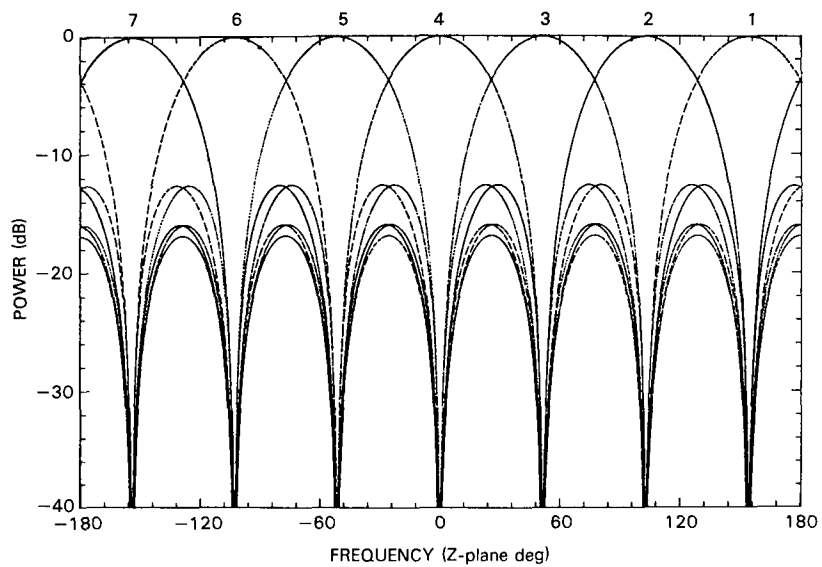


Fig. 7 — Plot of DFT filter subbands for seven taps

to a tapped delay line, such that we arrive at the overall system schematic illustrated in Fig. 8. The individual subband adaptive weights  $W_k$  are computed from the simple relationship for a pair of signals [13],

$$W_k = - \frac{\sum_{n=0}^N \hat{S}_k(\omega_n) \hat{V}_k^*(\omega_n)}{\sum_{n=0}^N |\hat{V}_k(\omega_n)|^2} \quad (4)$$

where  $(N + 1)$  is the total number of data samples,

$\hat{S}_k(\omega_n)$  is the  $k$ th subband output, main, and

$\hat{V}_k(\omega_n)$  is the  $k$ th subband output, auxiliary.

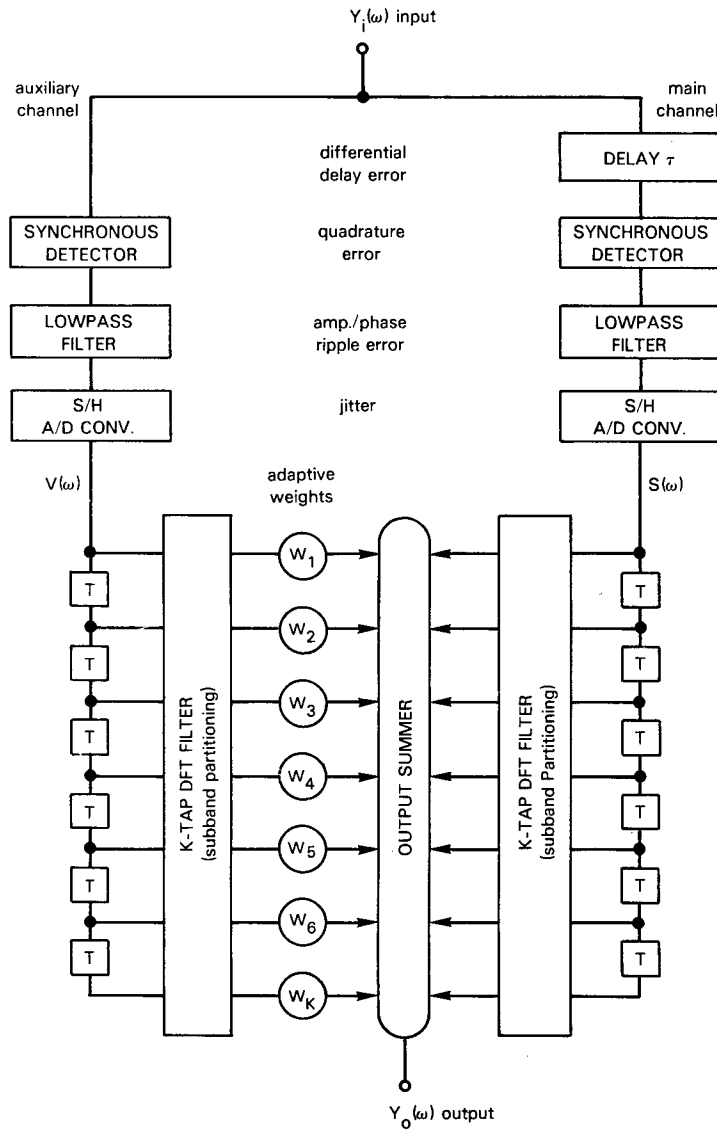


Fig. 8 — Multiple weight canceler using DFT filter subband partitioning, with one adaptive weight per subband

The subband outputs derive from the DFT operations,

$$\hat{\mathbf{S}}(\omega_n) = \mathbf{B}'\mathbf{S}(\omega_n) \quad (5)$$

$$\hat{\mathbf{V}}(\omega_n) = \mathbf{B}'\mathbf{V}(\omega_n) \quad (6)$$

where  $\mathbf{S}(\omega_n)$  and  $\mathbf{V}(\omega_n)$  are the main and auxiliary input vector signals to the DFT, and  $\hat{\mathbf{S}}(\omega_n)$  and  $\hat{\mathbf{V}}(\omega_n)$  are the main and auxiliary subband output vector signals resulting from the DFT operation.  $t$  denotes a matrix transpose. The DFT transformation matrix  $\mathbf{B}$  has individual row-column matrix elements containing discrete phase-shifts of the form,

$$b_{mk} = \frac{1}{\sqrt{K}} \exp \left[ \frac{2\pi}{K} \left( k - \frac{K+1}{2} \right) \left( m - \frac{K+1}{2} \right) \right] \quad (7)$$

where  $m$  is the input tap index,  $k$  is the subband output index, and  $K$  is the total number of taps or subbands.

$$\mathbf{B} = \begin{bmatrix} b_{11} & b_{12} & & b_{1K} \\ b_{21} & b_{22} & & b_{2K} \\ b_{31} & b_{32} & & b_{3K} \\ \cdot & \cdot & \dots & \cdot \\ \cdot & \cdot & & \cdot \\ \cdot & \cdot & & \cdot \\ b_{K1} & b_{K2} & & b_{KK} \end{bmatrix} \quad (8)$$

Digital signals are used in the simulations, based on a "sweep" sequence of  $(N+1)$  frequencies stepped from  $-\pi$  to  $+\pi$  in the  $Z$ -plane. The  $n$ th frequency  $\omega_n$  may be expressed

$$\omega_n = -\pi + n \frac{(2\pi)}{N}, \quad (9)$$

where  $n = 0, 1, 2, 3, 4, \dots, N$ . Note the direct relationship to  $\omega$  as defined for Eq. (1). Each unit-amplitude signal is given a random start-phase, such that we have a digital equivalent of clipped wide-band noise input. This swept noise-like signal characteristic is evidenced in Fig. 5(c) because quadrature error cancellation degradation happens to be sensitive to the particular phases of the individual signals. (The reader may verify this phase sensitivity with the help of Fig. 4.)

The canceler output  $Y_o(\omega)$  is the summation of subband adapted outputs,

$$Y_o(\omega) = \frac{1}{\sqrt{K}} \sum_{k=1}^K \left[ \hat{S}_k(\omega) + W_k \hat{V}_k(\omega) \right]. \quad (10)$$

If no errors are present, then Eq. (4) results in all  $W_k = -1$  and perfect cancellation occurs across the entire filter bandwidth.

Figure 9 illustrates the cancellation degradation for the various types of errors. In Fig. 9(a), a delay error of  $\tau = 1.0$  sampling period has been inserted in the main channel, and the response is plotted for  $K = 1, 7,$  and  $15$  DFT subbands. We note that the performance improves as  $K$  increases, but it is evident that DFT subband cancellation is seriously degraded by this type of error. In Fig. 9(b), amplitude ripple error of  $0.1$  peak and  $2.5$  cycles has been inserted in the auxiliary channel for  $K = 1, 7,$  and  $15$ . Here again, the degradation does improve as  $K$  increases, but the ripple error remains serious. In Fig. 9(c), synchronous detector quadrature errors of  $2.5^\circ$  have been inserted in the main and auxiliary channels (total of  $5^\circ$ ) for  $K = 1, 7,$  and  $15$ . Quadrature error degradation remains essentially constant vs frequency and cannot be improved by increasing the number of subbands. Performance is about  $6$  dB better than Fig. 5(c) only because the weights here are adaptive and compensate for half of the quadrature error. Figure 9(d) illustrates the behavior for a jitter error with uniform random distribution between peak values of  $\pm 2^\circ$ , added independently to I and Q signals in both channels. Jitter error degradation is similar to quadrature error in that it cannot be improved by increasing the number of subbands. Note the similarity to Fig. 5(d).

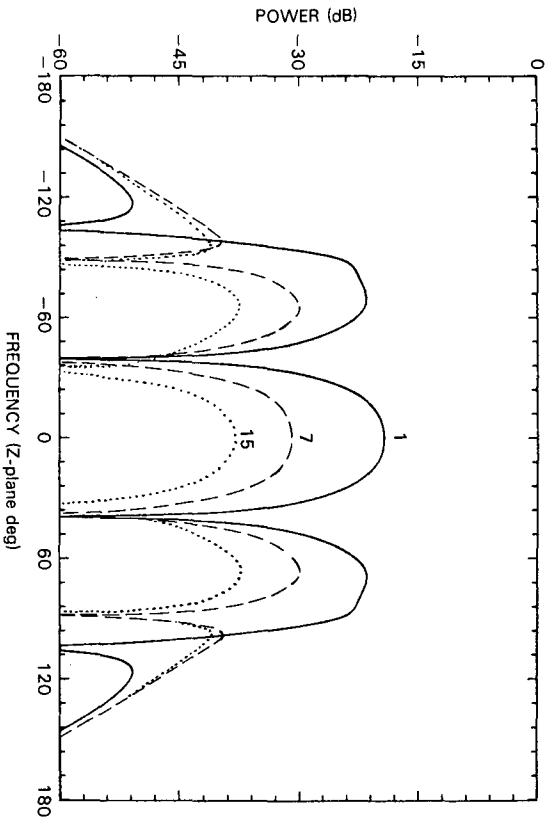
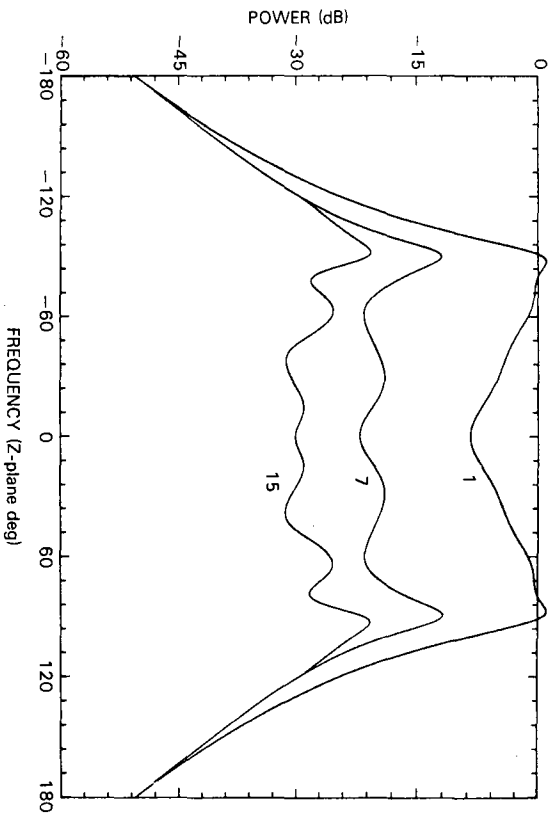
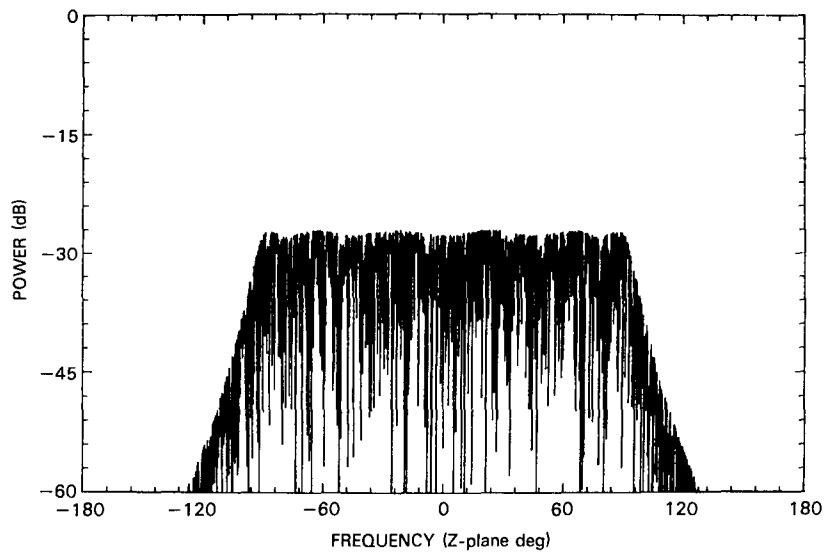
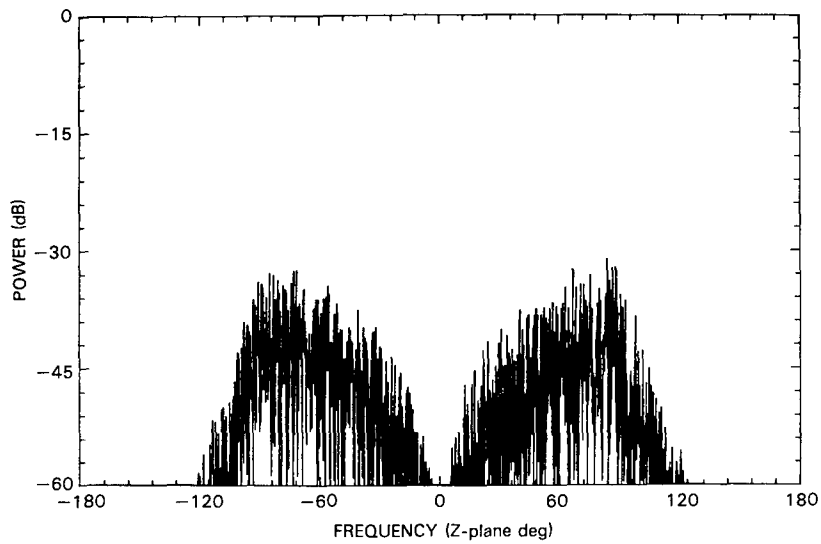


Fig. 9 — Cancellation degradation for various errors. DFT subband canceler, plotted for 1, 7, and 15 subbands



(c) Synchronous detector quadrature error of  $5.0^\circ$



(d) Random jitter error of  $2.0^\circ$  peak, both I&Q

Fig. 9 (Continued) — Cancellation degradation for various errors, DFT subband canceler, plotted for 1, 7, and 15 subbands

Note that for the purposes of this investigation, we deliberately have not taken an inverse DFT at the output, as would be necessary to obtain a final output pulse in the time domain. Rather, the investigation of cancellation behavior has been restricted to the frequency domain.

**TRANSVERSAL FILTER CANCELER**

The second multiple-weight digital filter to be examined is a transversal filter canceler (TFC), shown in Fig. 10. This circuit is identical in configuration to a one-step linear prediction filter and, also, to the generic "sidelobe canceler" [14]. The optimal weights may be arrived at by any of the current adaptive processing algorithms, with the choice determined primarily by system performance requirements. For our investigation purposes, it was convenient to employ the familiar sidelobe canceler algorithm based on a covariance matrix inverse [3],

$$\mathbf{W} = \mathbf{R}^{-1} \mathbf{\Lambda} \tag{11}$$

where  $\mathbf{W}$  is the adaptive weights vector for the TFC,  $\mathbf{R}$  is the signal covariance matrix, and  $\mathbf{\Lambda}$  is the equivalent "steering vector."

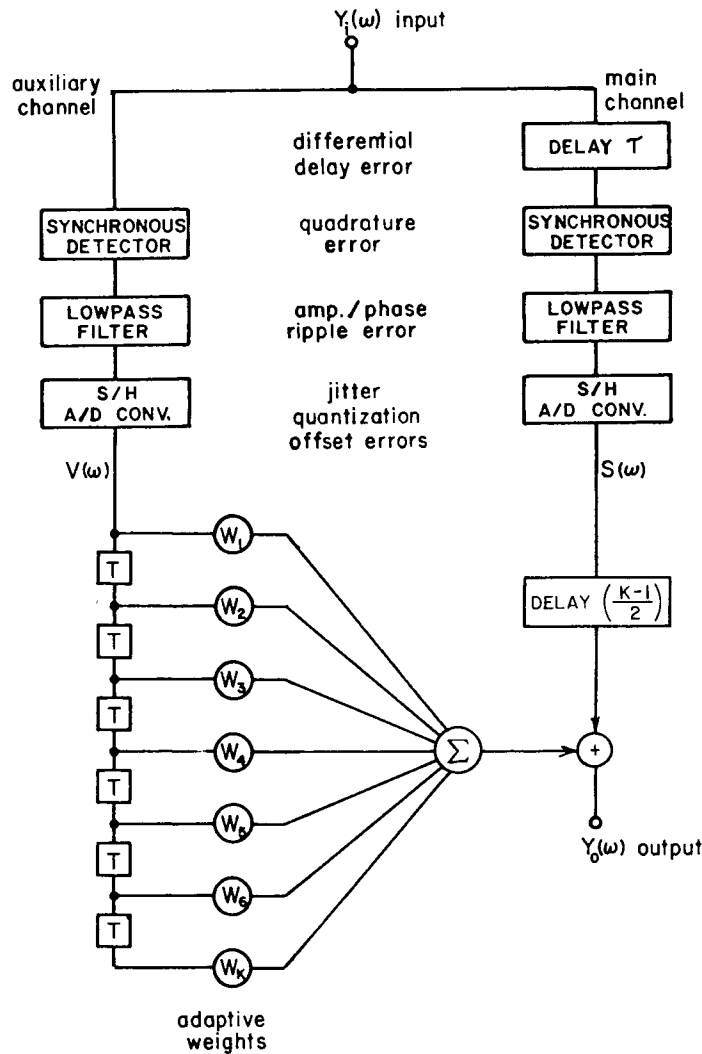


Fig. 10 — Multiple weight canceler using transversal filter, with one adaptive weight per delay line tap

$$\mathbf{\Lambda} = \frac{1}{(N+1)} \sum_{n=0}^{\Lambda} S_m(\omega_n) \mathbf{V}^*(\omega_n) \quad (12)$$

$$\mathbf{R} = \frac{1}{(N+1)} \sum_{n=0}^{\Lambda} \mathbf{V}^*(\omega_n) \mathbf{V}'(\omega_n) + \delta^2 \mathbf{I} \quad (13)$$

where  $S_m(\omega_n)$  is the main channel signal at the output summer,  $\mathbf{V}(\omega_n)$  is the auxiliary signal vector from the tapped delay line,  $\delta^2$  represents a small "pseudonoise" power term of  $-60$  dB level to facilitate matrix inversion,  $\mathbf{I}$  is the identity matrix, and  $\omega_n$  is the  $n$ th frequency defined in Eq. (9).

$$\begin{aligned} S_m(\omega_n) &= S(\omega_n) e^{-j\omega_n m} \\ V_k(\omega_n) &= V(\omega_n) e^{-j\omega_n(k-1)} \end{aligned} \quad (14)$$

where  $m = \left\lfloor \frac{K-1}{2} \right\rfloor$  is the midpoint index for the delay line,  $k$  is the delay line tap index,  $V(\omega_n)$  is the auxiliary channel signal input to the delay line,  $S(\omega_n)$  is the main channel signal that already incorporates differential delay error  $\omega_n \tau$ , if  $\tau \neq 0$ . Note that Eq. (14) implies unit delay between taps; i.e.,  $T = 1$ .

The TFC output is the summation of  $S_m(\omega)$  plus the weighted auxiliary delay line tap outputs,

$$Y_o(\omega) = S_m(\omega) + \sum_{k=1}^K W_k V_k(\omega). \quad (15)$$

If no errors are present, then all  $W_k = 0$  except for  $W_m = -1$ , and perfect cancellation occurs across the entire filter bandwidth for an odd number of taps.

Figure 11 illustrates the cancellation degradation for the various types of errors. In Fig. 11(a), a delay error of  $t = 1.0$  sampling period has been inserted in the main channel, and the response is plotted for  $K = 1, 4$ , and  $8$  delay line taps. The improvement in performance as  $K$  increases is far superior to the DFT filter (compare with Fig. 9(a)), despite the fact that an even number of taps represents the worst case for a TFC with  $\tau = 1.0$ . Note that for an odd number of taps where  $K > 3$ , the TFC gives perfect cancellation performance because there exists one tap for which the delay is precisely equal to the main channel delay. We expand upon this discussion of delay errors in the next section by comparing performance as a function of the delay-bandwidth product.

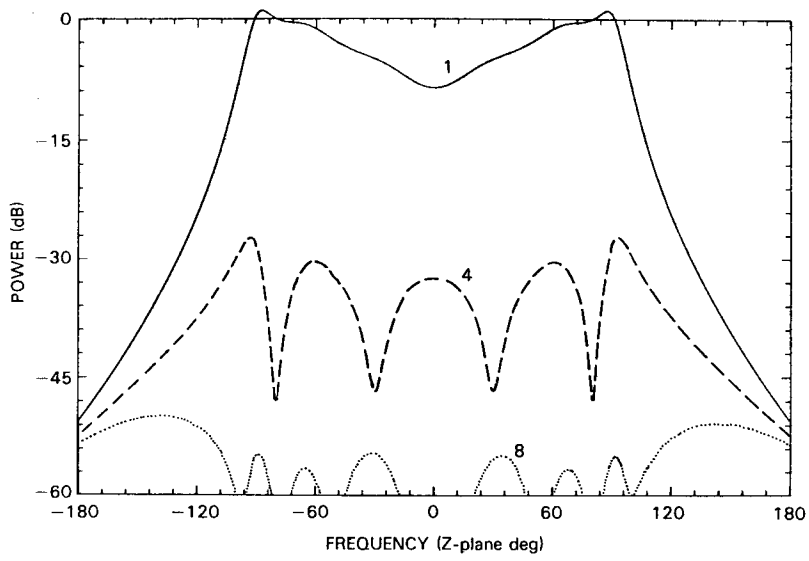
Figure 11(b) illustrates the degradation caused by an amplitude ripple error of  $0.1$  peak and  $2.5$  cycles, for  $K = 1$  and  $7$  delay line taps. Here again, the improvement in performance as  $K$  increases is far superior to the DFT filter (compare with Fig. 9(b)). What is demonstrated here is that the TFC uses its degrees of freedom (DOF) far more effectively within the lowpass filter bandwidth than does the DFT approach.

In Fig. 11(c), synchronous detector quadrature errors of  $2.5^\circ$  have been inserted in both the main and auxiliary channels (total of  $5.0^\circ$  error) for  $K = 7$ . Quadrature degradation remains essentially constant as  $K$  increases, except for a  $6$  dB ripple that appears across the passband (compare with Fig. 9(c)). Figure 11(d) illustrates the behavior for a jitter error with uniform random distribution between peak values of  $\pm 2.0^\circ$ , added independently to I&Q signals in both channels. Jitter error degradation is similar to quadrature error in that it cannot be improved by increasing the number of taps (compare with Fig. 9(d)).

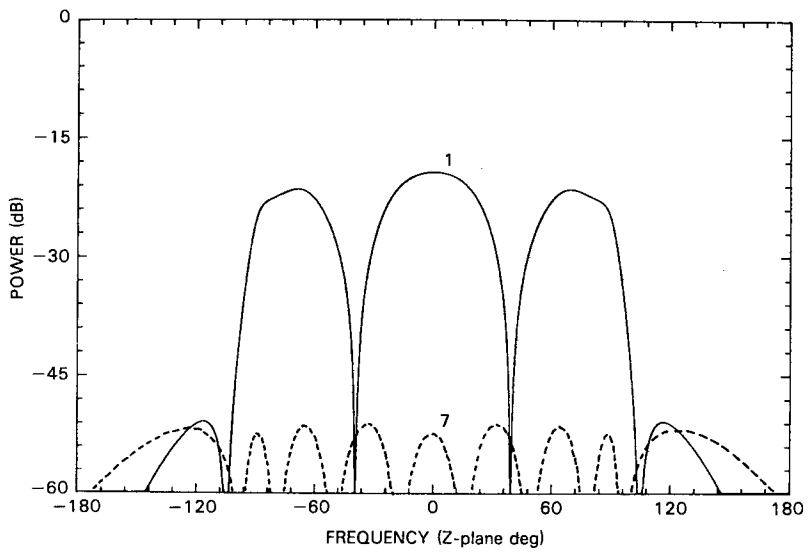
## FURTHER COMPARISON OF DFT VS TRANSVERSAL FILTERS

In the previous sections, we have noted the following comparisons between a DFT filter subband canceler and a transversal filter canceler (TFC) for these errors:

- Delay errors—TFC is far superior but requires additional performance criteria, such as odd vs even number of taps for a given  $\tau$ .



(a) Delay error of 1.0 sampling period, for 1, 4, and 8 taps



(b) Amplitude ripple error of 0.1 peak and 2.5 cycles

Fig. 11 — Cancellation degradation for various errors, transversal filter canceler, plotted for 1, 4, 7, or 8 taps

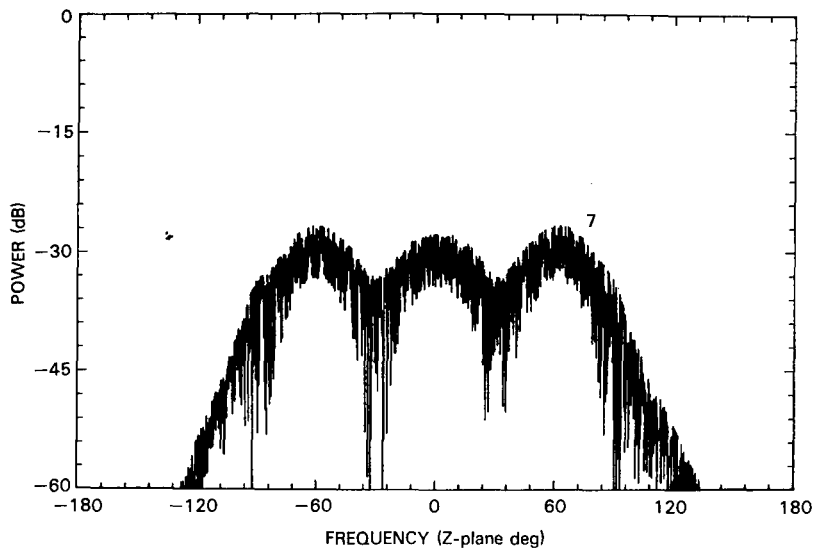
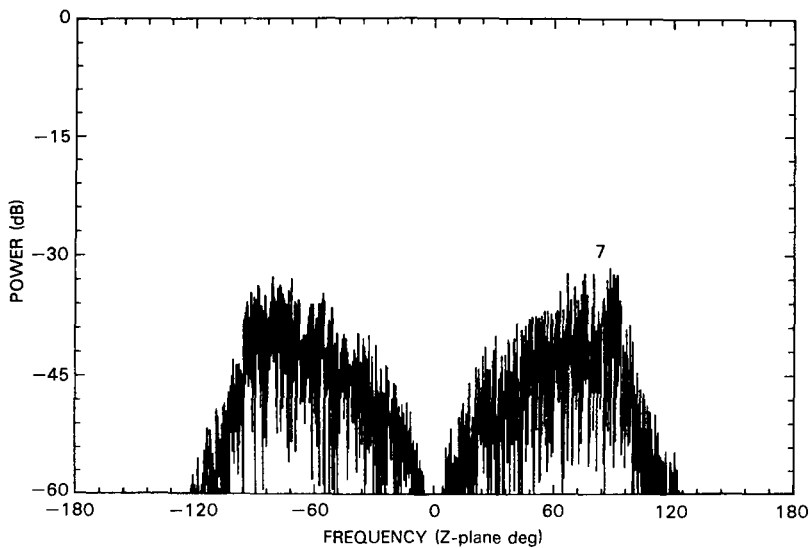
(c) Synchronous detector quadrature error of  $5.0^\circ$ (d) Random jitter error of  $2.0^\circ$  peak, both I&Q

Fig. 11 (Continued) — Cancellation degradation for various errors, transversal filter canceler, plotted for 1, 4, 7, or 8 taps

- Amplitude/phase ripple errors—TFC is far superior because of more effective use of its adaptive DOF.

- Quadrature error—Essentially no difference exists between DFT and TFC performance. This error cannot be removed via adaptation but, rather, requires calibration and I&Q signal correction in each channel.

- Jitter error—Essentially no difference exists between DFT and TFC performance. This error cannot be removed via adaptation and requires high-quality S/H components to keep the error as small as possible.

Of these, the delay error is examined in more detail in this section. We begin by demonstrating the significance of the lowpass filter in achieving good adaptive performance. Figure 12 shows the cancellation degradation resulting from a delay error of 0.5 sampling period, using  $K = 7$  subbands or taps,

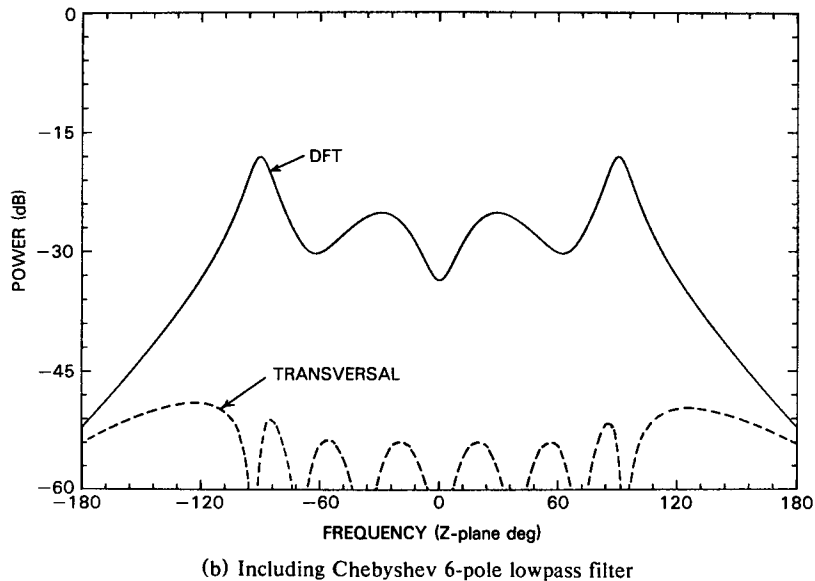
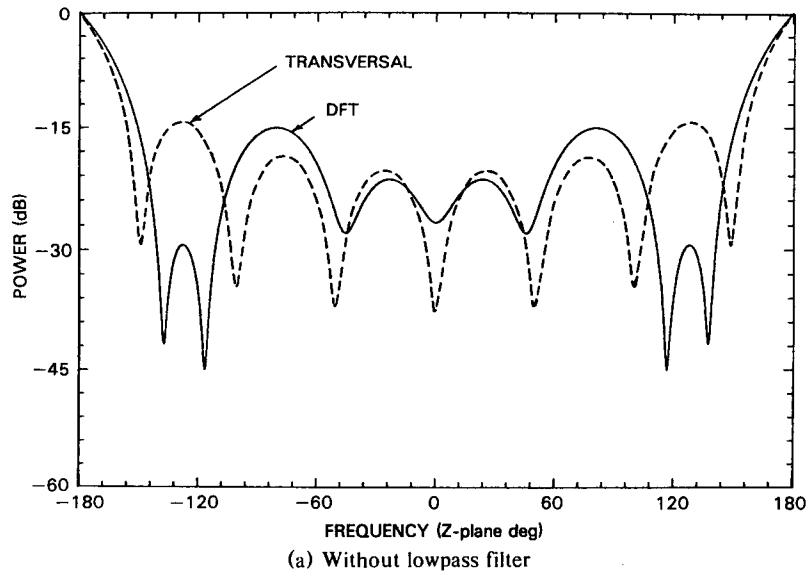


Fig. 12 — Cancellation degradation for delay error of 0.5 sampling period, both DFT filter and transversal filter, for  $K = 7$

when the lowpass filter is omitted or included. When omitted as in Fig. 12(a), there is little difference between DFT and TFC performance for this case and, in fact, both perform poorly. The poor performance occurs because our "clipped wideband noise" input fills the entire frequency range with this  $\omega\tau$  error. However, when our Chebyshev 6-pole lowpass filter of Fig. 2 is included as in Fig. 12(b), then the performance of the TFC improves dramatically across the passband. The DFT improves somewhat, but not nearly as much.

Perhaps the best further comparison criterion is to plot degradation performance vs delay-bandwidth product  $B\tau$ , where  $B$  is defined as the channel bandwidth normalized to the sampling rate. Such a plot is shown in Fig. 13 for an adaptive single weight, a DFT with  $K = 7$  subbands, and a TFC with  $K = 7$  taps. These plots are sensitive to the particular lowpass filter employed, and the data for Fig. 13 were taken with the Chebyshev 6-pole lowpass filter of Fig. 2 incorporated. The curves are derived from passband performance such as contained in Fig. 12(b) and, therefore, are approximate;

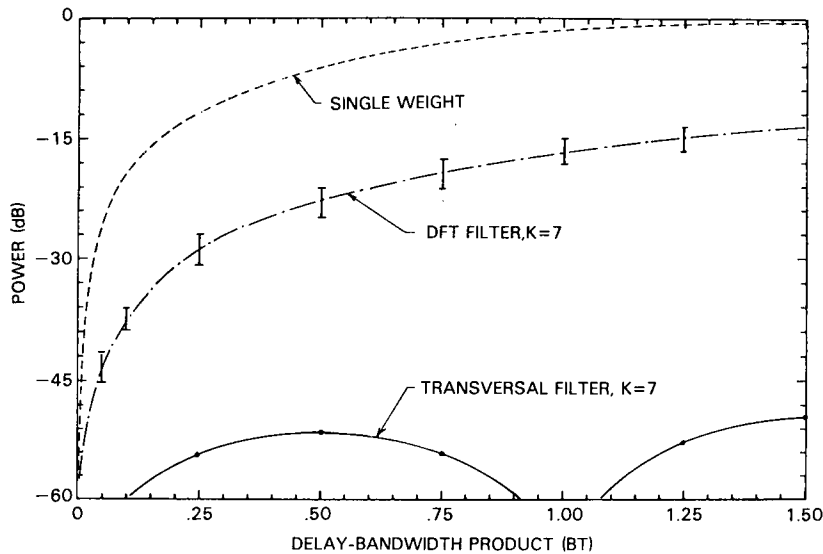


Fig. 13 — Cancellation degradation vs delay-bandwidth product, for adaptive single weight and multiple weight cancelers, using Chebyshev 6-pole lowpass filter

the indicated range for each point is an upper value of 3 dB below the highest peak, and a lower value equal to the next highest peak. Transversal filter performance is always cyclic vs  $B\tau$  product, having a  $\sin(\pi B\tau)$  behavior when  $K$  is odd and a  $\cos(\pi B\tau)$  behavior when  $K$  is an even number of taps. Performance improves as the value of  $K$  increases.

Figure 13 serves to emphasize the considerable performance superiority of the TFC in comparison with a DFT of the same  $K$  value.

## CONCLUSIONS

This investigation has shown that the TFC performance is generally far superior to the DFT sub-band system, for both differential delay errors and amplitude/phase passband ripple errors. This marked superiority is attributed to more effective use of its adaptive DOF and the fact that the TFC is inherently suited to differential delay compensation whereas the DFT is not. For quadrature errors and S/H jitter errors, there was essentially no difference in performance between the two.

## REFERENCES

1. P.W. Howells, "Explorations in Fixed and Adaptive Resolution at GE and SURC," *IEEE Trans.*, **AP-24**, 575-584, Sept. 1976.
2. P.W. Howells, "Intermediate Frequency Side-Lobe Canceller," U.S. Patent 3,202,990, Aug. 1965.
3. S.P. Applebaum, "Adaptive Arrays," *IEEE Trans.* **AP-24** 585-598, Sept. 1976.
4. O.L. Frost III, "An Algorithm for Linearly Constrained Adaptive Array Processing," *Proc. IEEE* **60**, 926-935, Aug. 1972.
5. L.E. Brennan, J.D. Mallet, and I.S. Reed, "Adaptive Arrays in Airborne MTI Radar," *IEEE Trans.*, **AP-24**, 607-615, Sept. 1976.
6. R.A. Monzingo and T.W. Miller, *Introduction to Adaptive Arrays* (John Wiley and Sons, New York, 1980).

7. D.R. Morgan and A. Aridgides, "Adaptive Sidelobe Cancellation of Wideband Multipath Interference," *IEEE Trans. AP-33*, 908-917, Aug. 1985.
8. B.L. Lewis and F.F. Kretschmer, Jr., NRL reports and communications of limited distribution dating back to Dec. 1976.
9. B. Widrow and S.D. Stearns, *Adaptive Signal Processing* (Prentice-Hall, Inc., Englewood Cliffs, NJ, 1985).
10. S.S. Narayan and A.M. Peterson, "Frequency Domain Least-Mean-Square Algorithm," *Proc. IEEE* **69**, 124-126, Jan. 1981.
11. G.M. Dillard, "Band Partitioning for Coherent Sidelobe Cancellation," Tech. Doc. 597, Naval Ocean Systems Center, May 1983.
12. O.V. Oppenheim and R.W. Schaffer, *Digital Signal Processing* (Prentice Hall, Englewood Cliffs, NJ, 1975).
13. W.F. Gabriel, "Building Block for an Orthonormal-Lattice-Filter Adaptive Network," NRL Report 8409, July 1980.
14. W.F. Gabriel, "Spectral Analysis and Adaptive Array Superresolution Techniques," *Proc. IEEE* **68**, 654-666, June 1980.